Supporting Information

Tailored Synthesis of Hollow Tubular In_2O_3/In_2S_3 Z-Scheme Heterojunctions for Highly Selective CO Production in CO_2 Hydrogenation

Fenghao Xing,[a] Qiutong Han*,[a] Lei Wang*,[a] Buyun Shi,[b] Chuqiu Wang,[a] Yichang Pan,[b]

[a] School of Physical and Mathematical Sciences, Nanjing Tech University, Nanjing 211816, PR China

[b] State Key Laboratory of Materials-Oriented Chemical Engineering, College of Chemical Engineering, Nanjing Tech University, Nanjing 211816, PR China

*Corresponding Authors E-mail:

hanqt@njtech.edu.cn.

wangl055@njtech.edu.cn

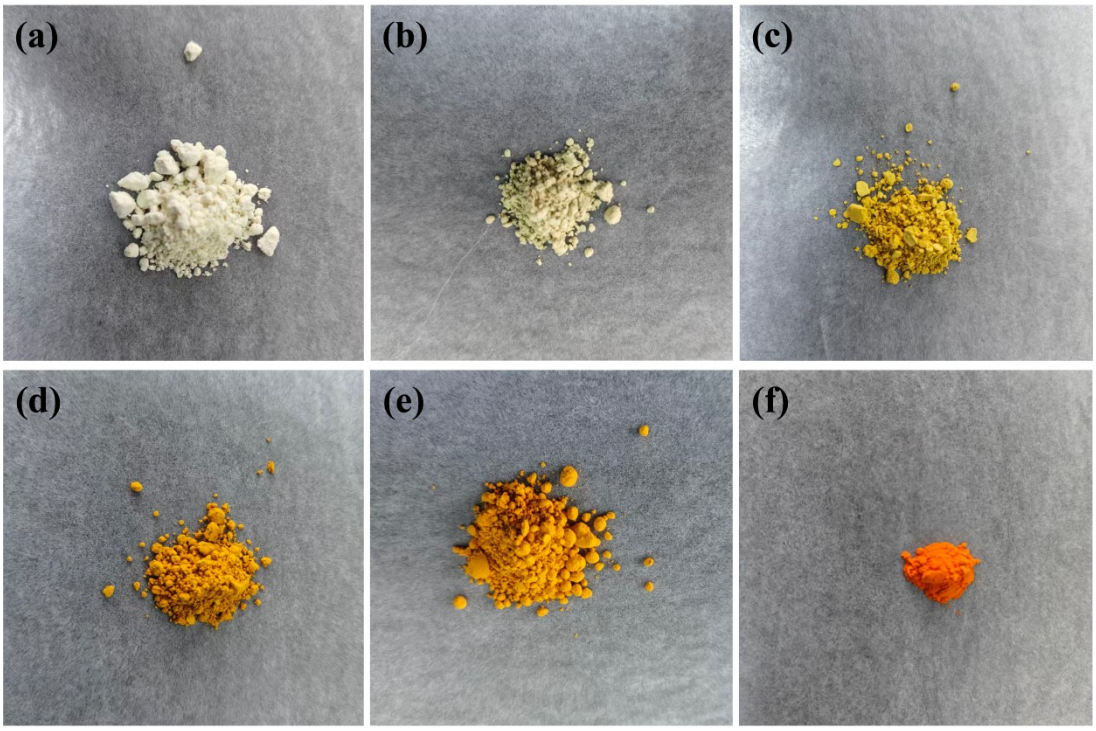

Figure S1. (a) In_2O_3, (b-e) IOIS-X (1, 2, 3, 4), (f) In_2S_3.

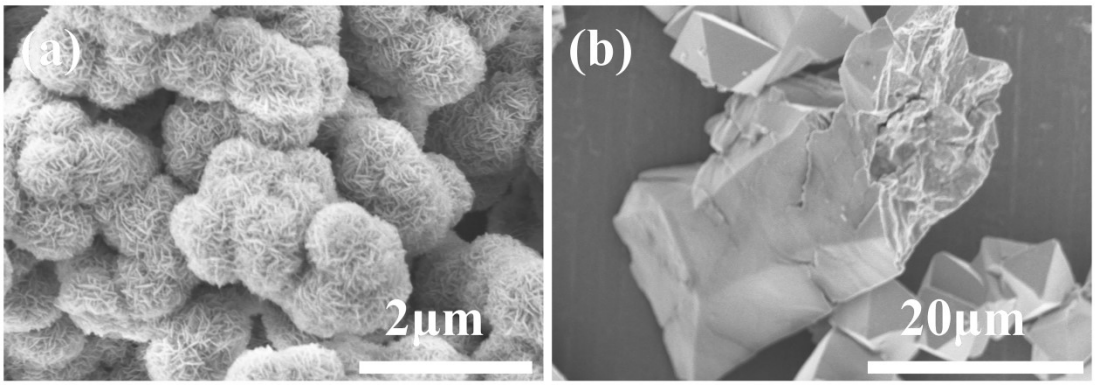

Figure S2. SEM images of (a) In_2S_3, (b) In_2O_3 SSR.

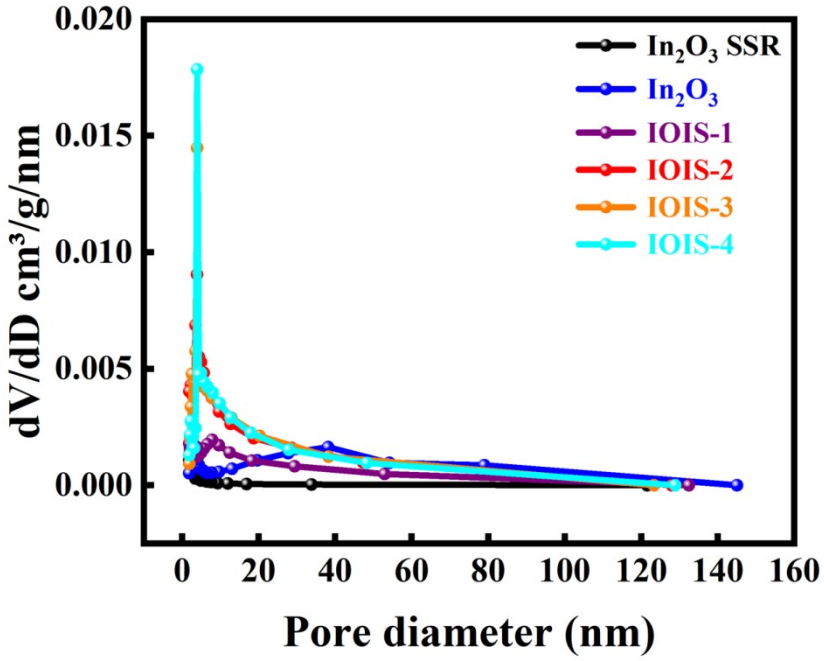

Figure S3. The pore size distribution of In_2O_3 SSR, In_2O_3, and IOIS-X. (X=1,2,3,4)

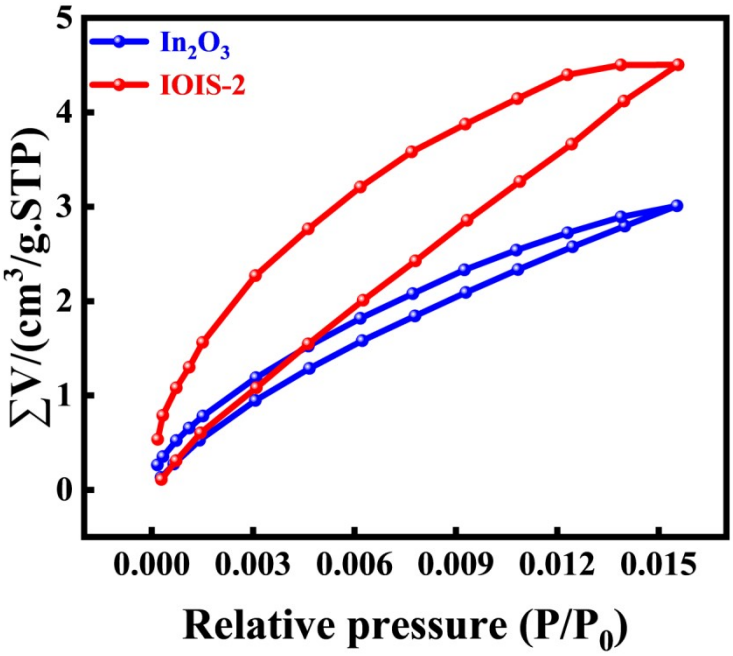

Figure S4. CO_2 adsorption isotherms of In_2O_3 and IOIS-2.

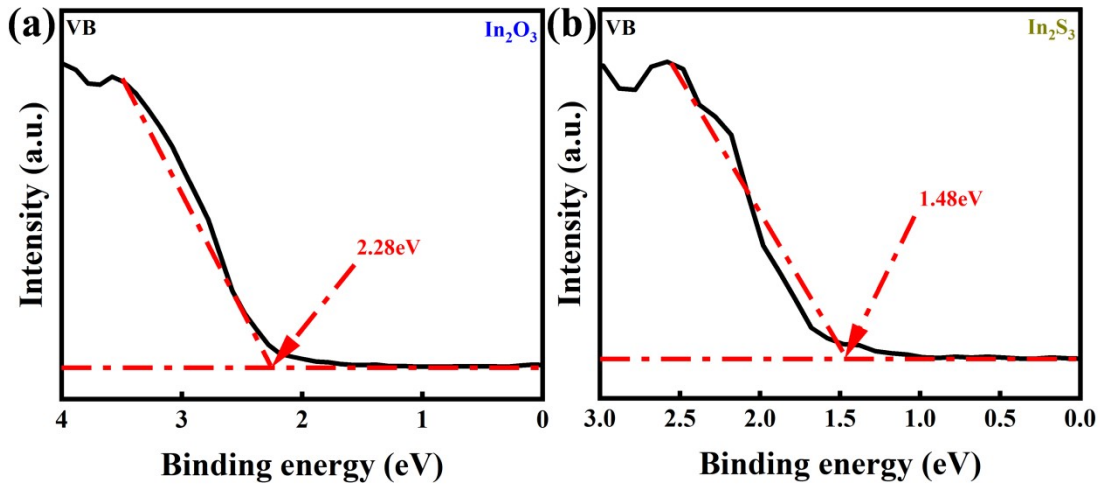

Figure S5. High resolution XPS valence band spectrum of (a) In_2O_3 and (b) In_2S_3.

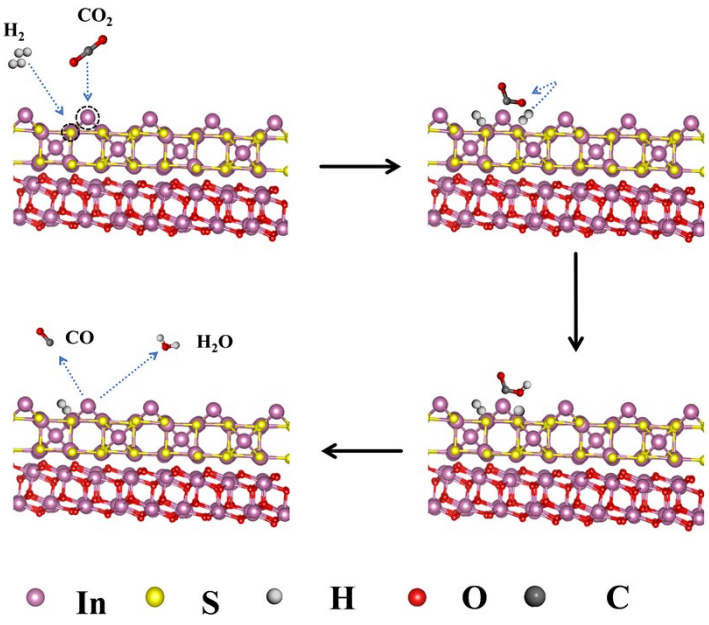

Figure S6. Catalytic mechanism diagram.

Based on previous studies and our preliminary characterization results, the adsorption and activation of CO_2 occur primarily on the In_2S_3 surface. It has been reported that the adsorption energies of CO_2 on In sites and S sites are -1.25 eV and -0.46 eV, respectively.[1,2] Among these, the coordinatively unsaturated surface In sites exhibit a more negative adsorption energy (i.e., stronger CO_2 adsorption capability), indicating that these sites serve as the active centers for CO_2 activation. Meanwhile, the adjacent surface S atoms are primarily responsible for the adsorption and dissociation of H_2, thereby promoting the subsequent hydrogenation of $*CO_2$ intermediates.

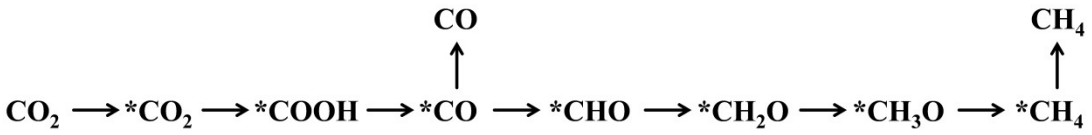

Figure S7. Reaction pathways for CO and CH_4 production on IOIS-2.

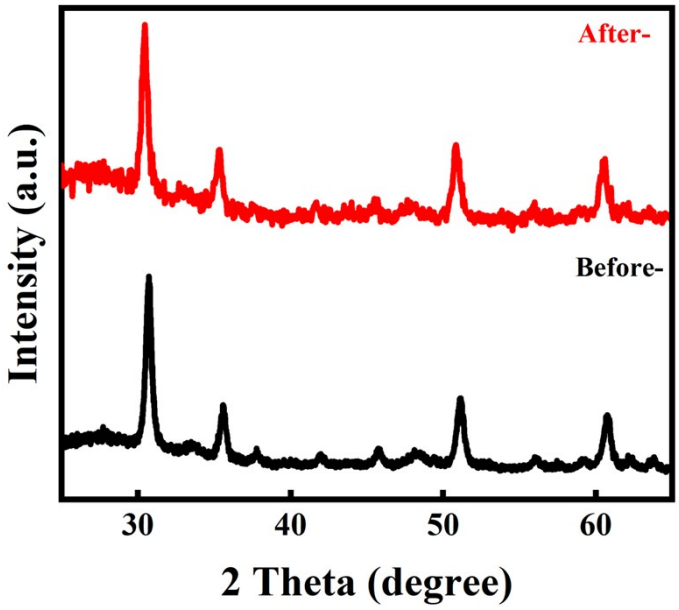

Figure S8. XRD patterns of IOIS-2 before and after the CO_2 reduction reaction.

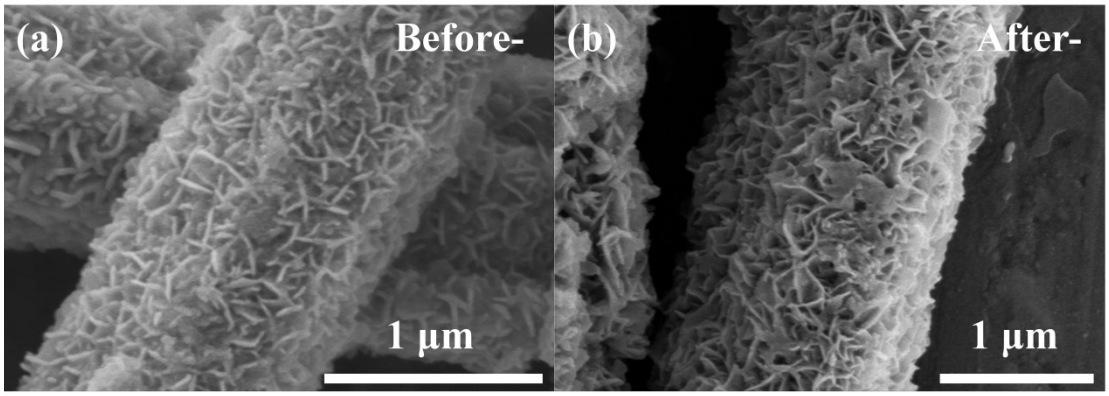

Figure S9. SEM images of IOIS-2 the photothermal catalyst (a) before and (b) after the CO_2 reduction reaction.

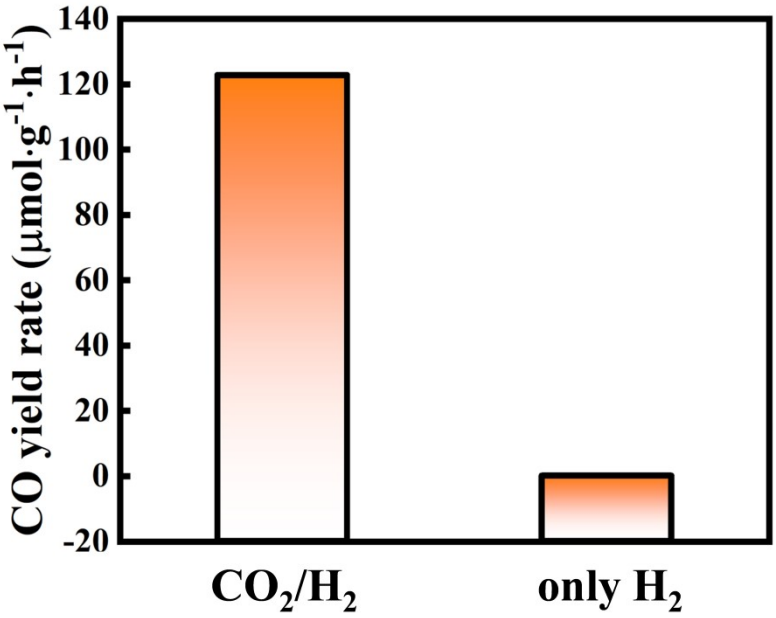

Figure S10. Comparison of CO production rates under CO_2-H_2 mixture and pure H_2.

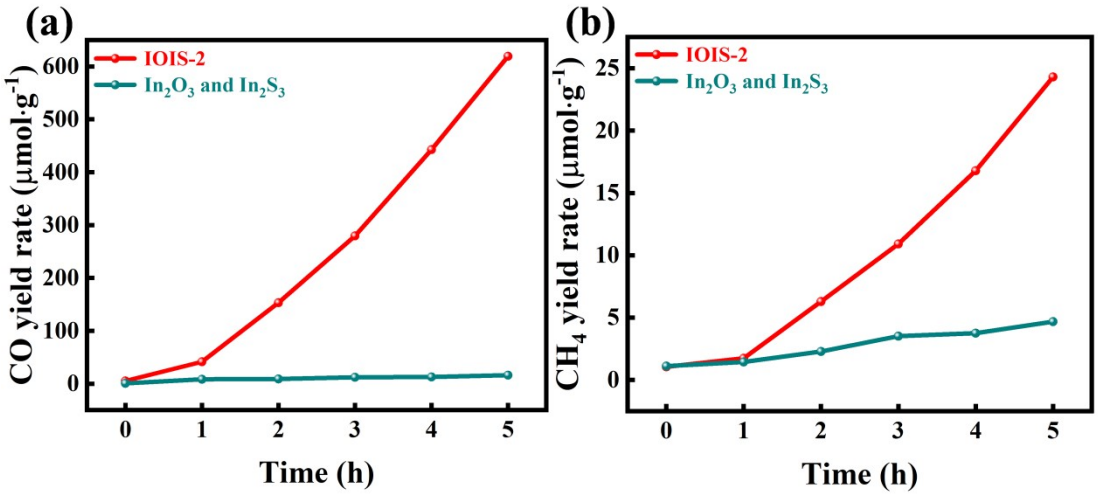

Figure S11. Comparison of CO generation rates between physical grinding and IOIS-2.

To validate the superiority of the Z-scheme heterojunction over a simple combination of the two materials, we prepared a physically mixed sample of In_2O_3 and In_2S_3 at the same mass ratio as IOIS-2 heterojunction. Under identical CO_2 reduction conditions, the physical mixture yielded CO and CH_4 production rates that are significantly lower than those of the Z-scheme heterojunction (Fig. S11). This result rules out any mechanical mixing effect and demonstrates that the intimate interfacial contact and directional Z-scheme charge transfer in the heterojunction are essential for promoting charge separation and utilizing the strong reduction potential required for efficient CO_2 reduction.

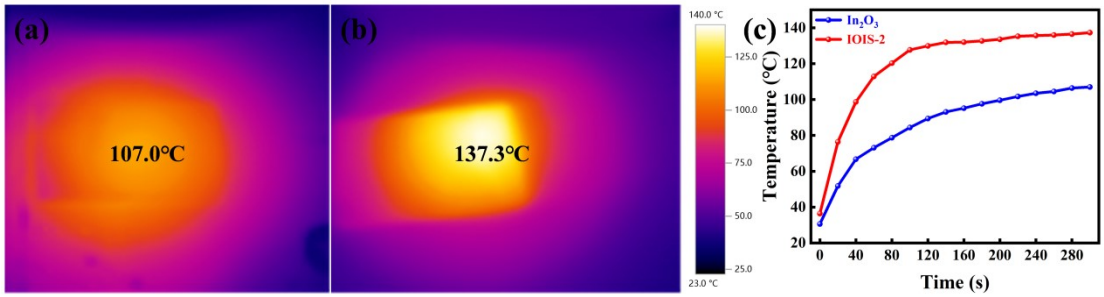

Figure S12. Surface temperatures of (a) In_2O_3 and (b) IOIS-2 under xenon lamp irradiation; (c) temperature variation at the initial irradiation stage.

The surface temperature of the catalysts was monitored by a Testo 865 thermal imager. After 5 min of illumination, the surface temperature of IOIS-2 reached 137.3 °C, notably higher than that of In_2O_3 (107.0 °C), confirming that the superior photothermal effect of IOIS-2 facilitates the photothermal CO_2 reduction reaction.

Table S1. A comparative study of catalysts for the hydrogenation of CO_2 to CO.

Catalyst	Rate/μmol·g^{-1}·h^{-1}	Selectivity/%	Temperature/℃	Pressure/MPa	CO_2/H_2	Refs
$In_2O_{3-x}(OH)_y$/SiNW	22	100	-	0.2	1	3
Fe@C/Ni_2P	179.90	96.86	200	-	-	4
$In_2O_{3-x}(OH)_y$ on Ni foam	755	100	295	0.1	1	5
V_4C_3-MXene	95.68	96	250	0.12	1/3	6
CoO_x/WO_{3-x}	26.07	79.88	25	0.1	-	7
3Cu-6Ni-Bi_2MoO_6	73.29	74.86	200	-	-	8
Fe@(N)C	13.29	~100	245	0.1	1	9
IOIS-2	122.80	96.35	180	0.1	3	This Work

References

1 Zhou, B.; Li. Z.; Xu, J.; Zheng, Y.; Zhang, Y.; Yuan, Y.; Yan, Y.; Kou, J.; Zhou, X.; Du, J.; Wu, X.; Shen, Q.; Zou, Z.; Zhou, Y. *ACS Appl. Nano Mater*. 2025, **8**, 12314-12321.

2 Wang, K.; Hu, Y.; Liu, X.; Li, J.; Liu, B. *Nat. Commun.* 2025, **16**, 2094.

3 Hoch, L. B.; O'Brien, P. G.; Ali, F. M.; Sandhel, A.; Perovic, D. D.; Mims, C. A.; Ozin, G. A. *ACS Nano*. 2016, **10**, 9017-9025.

4 Zhu, P.; Geng, M.; Qin, S.; Cao H.; He, Z.; Gao, X.; Wang, C. *Surf. Interfaces.* 2024, **46**, 104032.

5 Hurtado, L.; Mohan, A.; Ulmer, U.; Natividad, R.; Tountas, A. A.; Sun, W.; Wang, L.; Kim, B.; Sain, M. M.; Ozin, G. *A. Chem. Eng. J.* 2022, **435**, 134864.

6 Liu, Y.; Tan, G.; Feng, S.; Zhang, B.; Liu, T.; Wang, Z.; Bi, Y.; Yang, Q.; Ren, H.; Lv, L.; Liu, W.; Xia, A.; Zhao, Q. *Sep. Purif. Technol*. 2023, **326**, 124726.

7 Yang, J.; Tian, R.; Wang, D.; Dai, J.; Du, Z. *Acta Mater. Compos. Sin.* 2023, **40**, 5158-5169.

8 Guo, M.; Chen, Y.; Liu, J.; Qiu, J.;Wang, W.; Yang, Z. *Appl. Surf. Sci.* 2026, **730**, 166190.

9 Szalad, H.; Lu, P.; Primo, A.; Albero, J.; Garcia, H. *Chem. Commun.*, 2021, **57**, 10075.